Measurement of cross sections and asymmetry parameters for the production of charged pions from various nuclei by 585-MeV protons

J. F. Crawford, M. Daum, G. H. Eaton, R. Frosch, H. Hirschmann, R. Horisberger,* J. W. McCulloch,† and E. Steiner

SIN, Schweizerisches Institut für Nuklearforschung, Ch-5234 Villigen, Switzerland

R. Hausammann, R. Hess, and D. Werren‡

Département de Physique Nucléaire et Corpusculaire, Université de Genève, 32 bd. d'Yvoy, CH-1211 Genève, Switzerland

(Received 8 November 1979)

We have measured the differential cross section $d^2\sigma/d\Omega dT_\pi$ and the polarization parameter P for the production of π^+ and π^- in various target nuclei (^{1}H, ^{2}H, Be, C, O, Al, Ni, Cu, Mo, and Pb) by protons with a kinetic energy of 585 MeV, for production angles $\theta_\pi = 22.5°$, 45°, 60°, 90°, and 135°, and for pion kinetic energies T_π of 24, 35, 46, 88, 151, 192, and 254 MeV (all quantities in the laboratory system). Our data disagree strongly with recent data for 580-MeV protons. On the other hand, for pion energies up to 150 MeV, our cross sections differ little from those measured for a proton energy of 730 MeV. For nuclei with $A > 20$, the total production cross sections $\sigma(\pi^+)$ and $\sigma(\pi^-)$ show the $Z^{1/3}$ and $N^{2/3}$ proportionality expected from theoretical arguments. There is evidence in our data of a shift of the π^+ energy distributions compared to the π^- distributions due to the effects of the Coulomb field of the nuclear protons on the emitted pions.

[NUCLEAR REACTIONS ^{1}H, ^{2}H, Be, C, O, Al, Ni, Cu, Mo, Pb$(p, \pi^\pm)$, $T_p = 585$ MeV; measured $\sigma(T_\pi, \theta_\pi)$ and asymmetry parameter $P(T_\pi, \theta_\pi)$.]

I. INTRODUCTION

The main motivation for our measurements of pion production cross sections was to provide sufficient data to allow the optimal design of secondary pion and muon beams at SIN and other accelerator laboratories of similar proton energy. Although many groups have measured pion production cross sections,[1-18] only one experiment[17] at a proton kinetic energy $T_p = 730$ MeV has covered a wide variety of nuclei as well as a wide range of pion energies and production angles. The present experiment was carried out to produce a similar data coverage at $T_p = 585$ MeV as that of Ref. 17 at 730 MeV.

In addition to the differential cross section, the polarization parameter P for the pion production has been measured extensively for the first time in our experiment. We hope that the combined data will be useful for the improvement of theoretical models of pion production in nuclei. The "isobar" model of Silbar and Sternheim[19,20] reproduces accurately the measured ratios of the π^+ to π^- total production cross sections at 730 MeV (Ref. 17) and the dependence of the total production cross sections on nuclear size. For positive pions, the model[19,20] also reproduces fairly well the dependence of the differential production cross section $d\sigma/d\Omega$ on the production angle and, in addition, the pion energy distributions $d^2\sigma/d\Omega dT_\pi$ at fixed angles. However, for negative pions, the predictions of $d\sigma/d\Omega$ and $d^2\sigma/d\Omega dT_\pi$ are not satisfactory. Possible improvements to the model[19,20] will be discussed in Sec. V below.

II. EXPERIMENTAL METHOD

A. The proton beam

Our measurements were carried out in the pM1 polarized proton channel at SIN.[21] This beam is produced by scattering the unpolarized extracted proton beam in an 8 mm thick beryllium target through an angle of 8°. The scattered proton beam has a downwards transverse polarization of $(41.65 \pm 0.40)\%$.[22] Its intensity was typically 5×10^9 protons per second during our data taking. The kinetic energy of the proton beam was 585 MeV, with an absolute calibration uncertainty of 2 MeV (standard deviation) and an energy band $\Delta T_p/T_p$ of 0.4% full width at half maximum (FWHM). The position and profile of this beam near the pion production target were monitored continually throughout the experiment with an analog readout multiwire proportional chamber.[23] The dimensions of the beam spot at the pion production targets were 14 mm (FWHM) horizontally and 9 mm (FWHM) vertically. The transverse polarization of the beam could be rotated through 180° using a 1 m long superconducting solenoid situated along the beam line. This solenoid generated a longitudinal mag-

netic field of 4.5 T along the beam direction (see Fig. 1). The intensity of the proton beam was monitored using a scintillation telescope P_1P_2 detecting particles scattered at 30° to the beam direction from a 5 mm thick CH_2 target. The calibration between the telescope rate and the proton beam intensity was made after reducing the latter by a factor of 10^3 to 10^4. This was achieved by detuning a quadrupole magnet upstream of the acceptance-defining slit system of the beam channel. Thus the intensity of the beam could be reduced without changing the beam dimensions at the pion production targets. A direct measurement of the beam intensity at this position could then be made with a scintillation counter of dimensions $50\times50\times15$ mm^3 placed in the beam and compared directly with the P_1P_2 rate. This calibration was carried out at frequent intervals during the experiment for both conditions of the precession solenoid (i.e., for down and up directions of the beam polarization). Different calibrations were expected because of the dependence of the scattering cross sections from the CH_2 target on the direction of the beam polarization; however, for each solenoid condition, calibrations consistent within the statistical uncertainties were obtained. The beam intensities for these measurements were varied from 4×10^5 to 1.1×10^6 protons per second. The following ratios of direct beam rate to telescope rate were obtained:

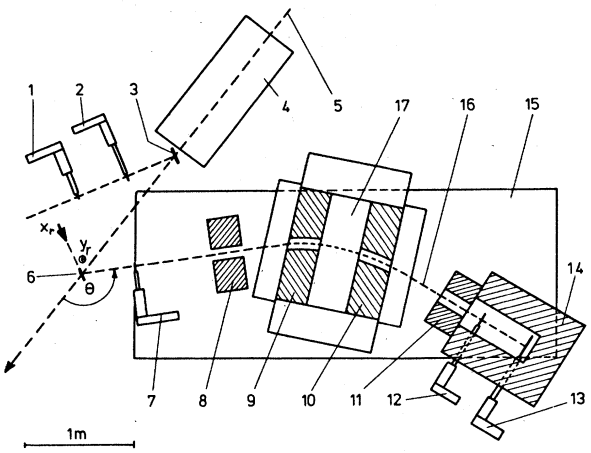

FIG. 1. Plan of the experimental arrangement: 1. scintillation counter P_2, 2. scintillation counter P_1, 3. CH_2 target for beam intensity measurement, 4. superconducting solenoid, 5. central trajectory of the incident proton beam, 6. pion production target, 7. scintillation counter π_1, 8–11. lead collimators, 12. scintillation counter π_2, 13. scintillation counter π_3, 14. lead shielding, 15. spectrometer turn table, 16. central trajectory of the spectrometer, 17. spectrometer magnet.

K = proton rate/P_1P_2 rate

$= (3.311\pm0.024)\times10^5$ for beam polarization up,

K = proton rate/P_1P_2 rate

$= (3.002\pm0.025)\times10^5$ for beam polarization down.

The quoted uncertainties in K are the statistical errors. The proton beam was focused onto a remotely controlled target ladder containing eleven different materials (see Sec. III). The angle α between the normal to the target and the proton beam was adjusted according to the pion production angle under study. This angle α was set at $\theta_\pi/2$ for $\theta_\pi = 22.5°$, 45°, and 60° laboratory angles and $\alpha = \theta_\pi/2 + 90°$ for $\theta_\pi = 90°$ and 135° (see Ref. 24).

B. The pion spectrometer

The particles produced from the targets were momentum analyzed in a 1 m spectrometer magnet and their time of flight (TOF) through the spectrometer was determined using the scintillation counters π_1, π_2, and π_3 shown in Fig. 1. The TOF measurement between π_1 and π_2 allowed clear separation of electrons and pions produced from the target. The spectrometer was mounted on a table which could be rotated about a vertical axis through the center of the target system. The magnet included precisely machined and positioned lead collimators as shown in Fig. 1. The acceptance solid angle $\Delta\Omega(p)$ of the spectrometer is

$$\Delta\Omega(p) = \iint \Delta\Omega(p, x_r, y_r) f(x_r, y_r)\, dx_r dy_r ,$$

where $\Delta\Omega(p, x_r, y_r)$ is the solid angle of the spectrometer for particles generated from the target point x_r, y_r with a momentum p, and $f(x_r, y_r)$ is the distribution function of the pion source; the integral of $f(x_r, y_r)$ over the (x_r, y_r) plane is unity. The x_r and y_r axes are indicated in Fig. 1. The acceptance solid angle was calculated using a Monte Carlo program for isotropically distributed initial flight directions of the particles produced from the target and for a typical distribution function $f(x_r, y_r)$. The result is shown in Fig. 2. The asymmetrical form of this resolution curve results in an average momentum 1.5% higher than the momentum p_0 of a particle traveling along the central trajectory of the spectrometer. The accepted momentum band of the spectrometer $\Delta p/p_0$ is 18.5% (FWHM).

C. The electronics

The signals for the TOF measurement were obtained from the counters π_1 and π_2 using the electronic system shown in Fig. 3. The counter π_3 was used to reduce the accidental coincidence rate. The flight path between the counters π_1 and π_2 was 355 cm. The light guide of the π_2 counter was at-

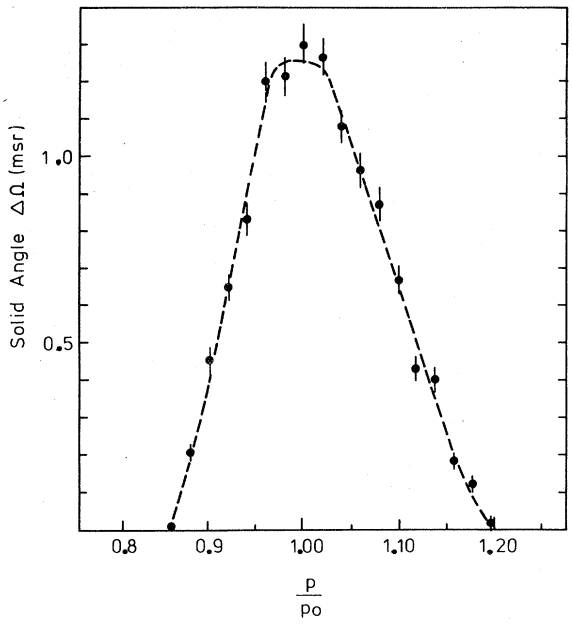

FIG. 2. Momentum resolution curve of the magnetic spectrometer, calculated with a Monte Carlo computer program. Abscissa: momentum of particles divided by the momentum for the central trajectory. Ordinate: acceptance solid angle of the spectrometer. The results of the Monte Carlo program are plotted as points with error bars. The curve has been drawn to guide the eye.

tached to the right hand side of π_2, an orientation partially compensating for the TOF difference between the low momentum pions incident on the right hand side of π_2 and the higher momentum pions on the left. The optimal TOF resolution was about 0.9 ns (FWHM). Typical TOF spectra are shown in Figs. 4 and 5. The pulses from the pion

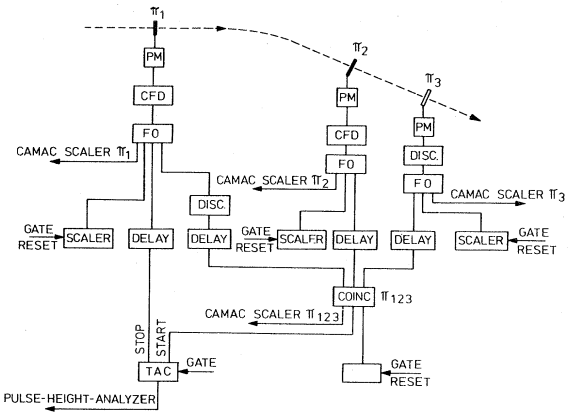

FIG. 3. Diagram of the electronics. π_1, π_2, π_3: scintillation counters (see Fig. 1), PM: photomultiplier, CFD: constant fraction discriminator, DISC: discriminator, FO: fan out, TAC: time-to-amplitude converter.

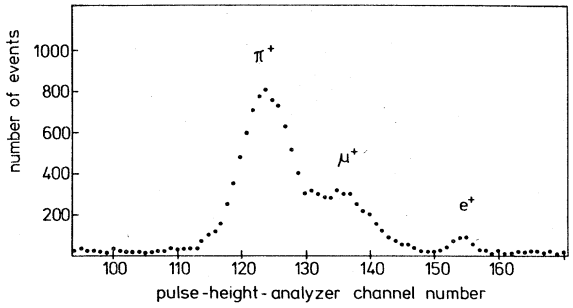

FIG. 4. Time-of-flight spectrum; $p_0 = 97$ MeV/c (see Fig. 2), π^+, $\theta_\pi = 90°$, target CH_2.

counters π_1 and π_2 were fed into constant fraction discriminators to preserve the good timing resolution. The output from the π_1 discriminator was used after suitable delay as the stop pulse for a time-to-amplitude converter (TAC), while the start pulse was generated from a coincidence between the three pion counters where the timing was defined by the counter π_2. The TAC output was processed by a CAMAC compatible 1000 channel pulse-height analyzer. At the end of each data-taking run, the pulse-height spectrum was read into a PDP 11/20 on-line computer, together with all the measured rates in the pion and proton counters. The experimental conditions for each run were fed into the computer before the start of data taking and all information was written on magnetic tape for subsequent analysis. The computer was also used to display the data at the end of each run and to carry out integrations of the TOF spectra.

III. DATA TAKING

A. Data coverage

We have measured pion production cross sections at the angles $\theta_\pi = 22.5°$, 45°, 60°, 90°, and 135° (lab system) with respect to the direction of

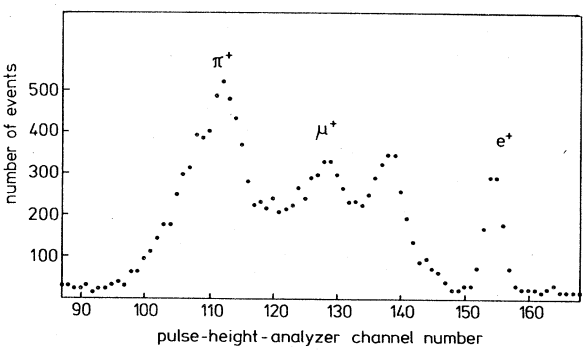

FIG. 5. Time-of-flight spectrum; $p_0 = 74$ MeV/c, π^+, $\theta_\pi = 60°$, target CH_2. The peak in channel 138 is due to fast pions which are scattered through the spectrometer.

the incident proton beam. At some of these angles data for incident proton energies similar to ours exist. The pion energies studied were: $T_\pi = 24$, 35, 88, 151, and 254 MeV at $\theta_\pi = 22.5°$; $T_\pi = 24$, 35, 88, 151, and 192 MeV at $\theta_\pi = 45°$; $T_\pi = 24$, 35, 46, 88, and 151 MeV at $\theta_\pi = 60°$, 90°, and 135°. Some of these energies were chosen such that they were near the pion energies in the reaction $pp \to d\pi^+$ at one of the angles used in the experiment (see Sec. V and Fig. 13). We used the target materials CH_2, C_6D_{12}, Be, C, Al, Al_2O_3, Ni, Cu, Mo, and Pb; the three materials CH_2, C_6D_{12}, and Al_2O_3 were used to determine the cross sections for the proton, the deuteron, and the oxygen nucleus, respectively. The liquid C_6D_{12} was contained in a cell with Mylar windows; an empty Mylar cell was used for the corresponding background measurements. For the targets other than C_6D_{12} the background was measured using an empty partition of the target ladder ("air" target). Thus we used twelve different targets. The pion production experiment consisted of 1200 separate runs (12 targets, 5 angles, 5 pion energies, 2 pion charge signs, and 2 signs of the proton beam polarization); one run lasted 200 to 600 sec.

B. Time-of-flight spectra

A typical time-of-flight spectrum is shown in Fig. 4. Since the start pulse was derived from the counter π_2 and the stop from π_1, our TOF spectra are reversed with faster particles at the right hand side of Fig. 4. The electrons occur always at the same TOF position of 11.7 ns between π_1 and π_2 (channel 154 in the displayed spectrum) irrespective of the momentum setting of the spectrometer. A peak in the TOF spectrum due to pions is observed at low channel numbers, while muons created before the spectrometer magnet fall between these pions and the electrons. Muons created after the spectrometer magnet cannot be distinguished by time of flight from the pions; this contamination was calculated with a Monte Carlo program (see Sec. IV). The random background in the TOF spectra was determined from the number of events outside the $\pi\mu e$ region. A time-of-flight spectrum at low momentum is shown in Fig. 5. It contains an additional peak near the electrons due to scattering of higher energy pions in the lead collimators of the spectrometer magnet. This peak is discussed in Sec. IV.

C. Measurement of the elastic proton-proton scattering

As a check of the momentum and solid angle acceptance of our spectrometer as well as the monitoring of the proton beam and the operation of the spin precession solenoid, we carried out subsidiary measurements of the proton-proton elastic scattering cross section and asymmetry. These data were taken at laboratory scattering angles of 45° and 60° using a CH_2-C difference method and high magnetic field settings of the spectrometer. The apparatus was the same as that used for the pion production measurements. In the TOF spectra there was an isolated peak due to protons accepted by the spectrometer.

IV. DATA ANALYSIS

In our data analysis, particle time-of-flight (TOF) spectra were generated with a Monte Carlo computer program, and compared with the experimental TOF spectra. The initial estimation of the differential cross section used in the Monte Carlo program in the case of the proton-proton scattering test was derived from the Saclay nucleon-nucleon phase shifts.[25] In the case of the pion production measurements, the data of Ref. 2 and a preliminary analysis of our own data[24] were used. Pions were generated in a large solid angle and momentum range to ensure that no decay muons were lost.

Other inputs for the Monte Carlo program were the properties of the incident proton beam and the production targets, the geometrical arrangement of the counters, the collimators, and the spectrometer magnet. The pion decay probabilities, nuclear and multiple scattering as well as energy loss of the particles in the production target, the air, the counters, and the collimators were included in the calculation.

The experimental TOF spectra were well reproduced by the Monte Carlo calculation in all cases; in particular, for low momentum settings of the spectrometer, the peaks like that around channel 138 of Fig. 5 were also present with correct position, shape and height, within statistics, in the Monte Carlo TOF spectra. These peaks in the Monte Carlo TOF spectra were seen to be due to high energy pions inscattered from the collimators through the spectrometer. The ratio of inscattered to direct pions in the TOF spectra (an inscattered particle has touched one of the lead collimators shown in Fig. 1) was much smaller at higher momentum settings of the spectrometer. However, at low momentum settings (such that $T_\pi \leq 46$ MeV at the target center), the inscattered pions in the direct pion TOF peak contribute only about 5%, whereas for settings with $T_\pi > 88$ MeV the inscattered pions fall in the direct pion peak and contribute typically 15% of all the pion events in this peak.

In the case of the p-p scattering, there were at the peak of the Monte Carlo distribution shown in

Fig. 17, i.e., at 8.5 kG, (88.9 ± 4.7) direct and (7.8 ± 1.4) inscattered protons per 10^8 primary protons in the peak of the Monte Carlo TOF spectrum (most inscattered protons had a TOF in the peak region). The Monte Carlo pion and muon TOF spectra were compared with the measured spectra (see Figs. 4 and 5), from which the random background had previously been subtracted. A scaling factor was obtained by dividing the number of events in the pion peak of the experimental spectrum by that of the theoretical spectrum. This "pion peak" contains a contamination of 10 to 20% "late muons" born after the spectrometer magnet. The parents of the late muons were pions with kinematical properties similar to those of the accepted pions. Therefore the scaling factor was used to correct the initial estimation of the cross section for the central production angle and the average initial kinetic energy of the pions accepted by the spectrometer. The polarization parameters were calculated from a comparison of the number of events in the experimental pion or scattered proton peak in the TOF spectra for both directions of the beam polarization.

V. RESULTS

The measured pion production cross sections $d^2\sigma/d\Omega\, dT_\pi$ are presented in Figs. 6–10. Table I shows our data for carbon.[26] It also includes the measured data on electron contamination and the polarization asymmetry in pion production. The quoted uncertainties are due to the statistical errors in the experimental and theoretical TOF spectra; the uncertainty of the integration limits for the pion peaks are also included. However, the quoted uncertainties do not include a number of systematic effects.[24] The uncertainty due to the monitoring of the proton beam intensity, common to all the cross sections $d^2\sigma/d\Omega\, dT_\pi$, is estimated to be 3%. A further uncertainty arises from the Monte Carlo calculation of the direct muon and inscattered pion and muon contribution to the direct pion TOF peak (see Sec. IV). This uncertainty of $d^2\sigma/d\Omega\, dT_\pi$ is estimated to be 5%. The quadratic sum of the estimates of all systematic uncertainties is 7% (one standard deviation).

Because of the large momentum acceptance of the spectrometer used in the experiment, the cross sections and asymmetries quoted in Table I are average values over fairly large regions of pion kinetic energies, namely (24 ± 3), (35 ± 5), (46 ± 7), (88 ± 12), (151 ± 20), (192 ± 25), or (254 ± 31) MeV. The asymmetry parameter P is defined as $P = (\sigma_{up} - \sigma_{down})/(\sigma_{up} + \sigma_{down})$, for a proton beam fully polarized in the direction perpendicular to the pion production plane. Here σ_{up} is the differential pion production cross section for beam protons with spin up and for pions emitted to the left, while σ_{down} is the same for beam protons with spin down. Thus the "up" direction is defined as usual by $\vec{n} = \vec{k}_p \times \vec{k}_\pi / \sin\theta_\pi$, where $\vec{k}_p$ and $\vec{k}_\pi$ are unit vectors in the direction of the proton and pion mo-

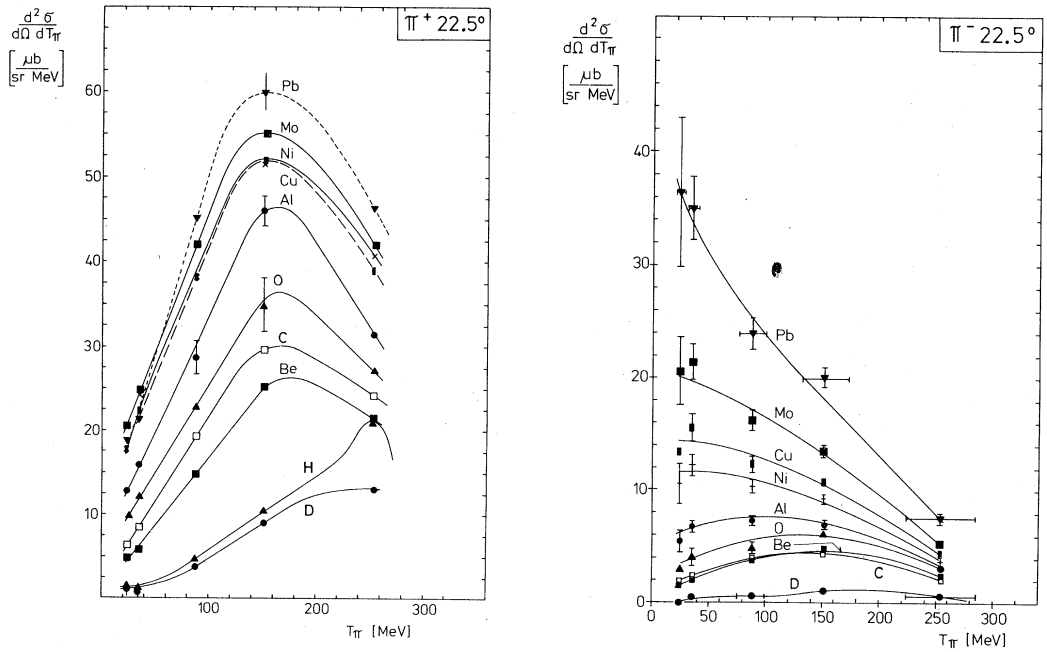

FIG. 6. Measured pion production cross sections for π^+ and π^- at a production angle θ_π of 22.5°.

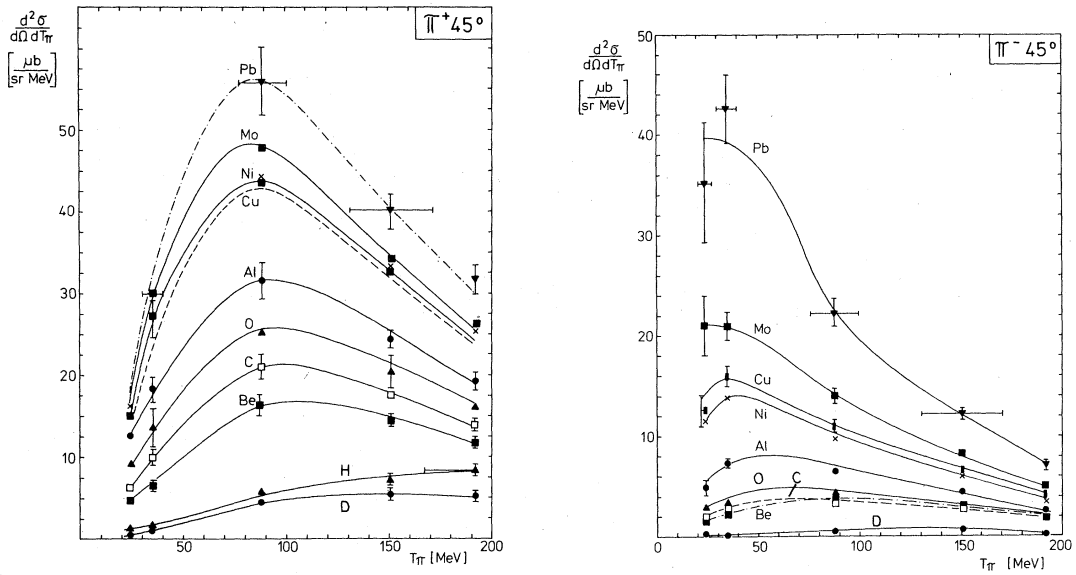

FIG. 7. As Fig. 6: production angle $\theta_\pi = 45°$.

mentum.

The ratio of particle rates $e/(\pi+\mu_l)$, quoted in Table I, was observed in a scintillator telescope. The particle flight path from the pion production target to this telescope was 4.5 m long. Here μ_l (late muons) are muons which originated from pion decays downstream from the pion spectrometer magnet. These muons were not separated from the pions in our time-of-flight spectra. A Monte Carlo calculation showed that the rate of late muons was in all cases smaller than about one fifth of the pion rate. The pion production targets were plates 5 cm high, 7 cm wide, and about 1 g/cm^2 thick. The normal $\vec{N}$ to the target face lay in the pion production plane. The angle α between the normal $\vec{N}$ and the proton beam was $\alpha = \theta_\pi/2$ for

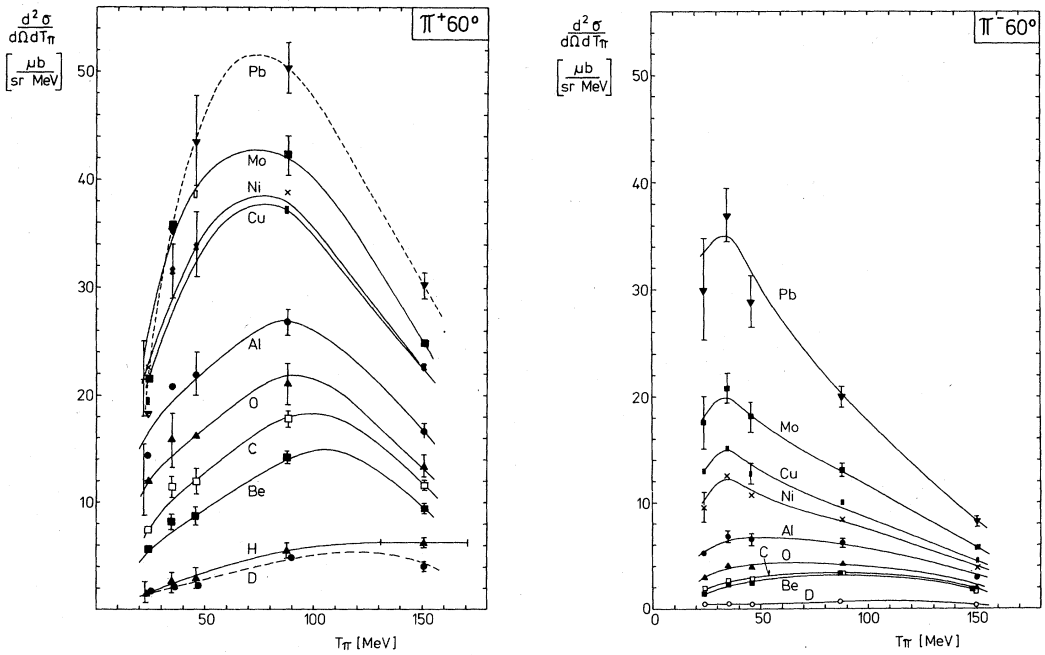

FIG. 8. As Fig. 6: production angle $\theta_\pi = 60°$.

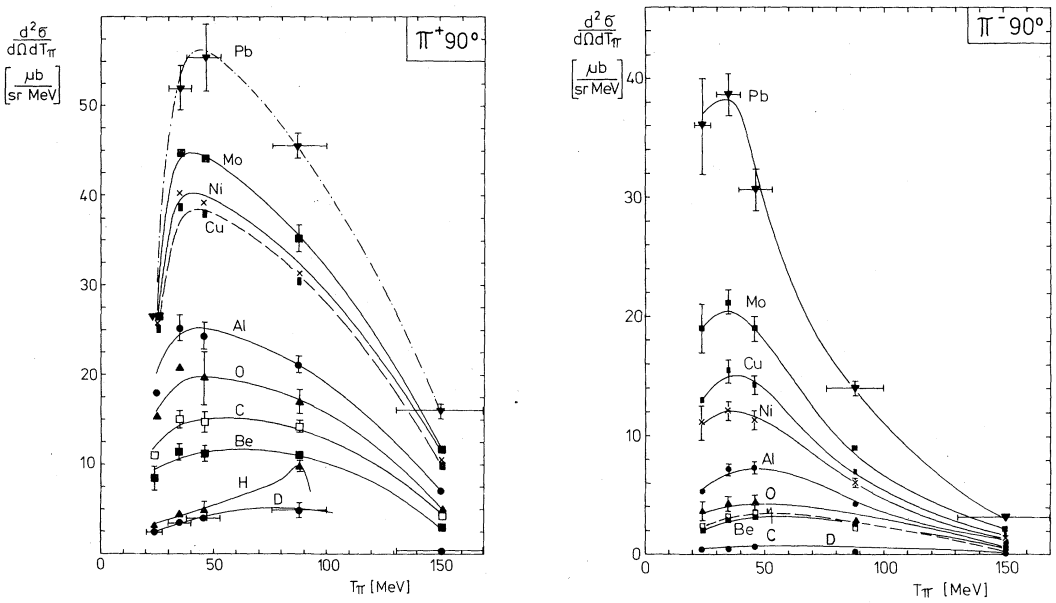

FIG. 9. As Fig. 6: production angle $\theta_\pi = 90°$.

$\theta_\pi = 22.5°$, 45°, and 60°. For $\theta_\pi = 90°$ and 135° the angle was $\alpha = (\theta_\pi/2) + 90°$.

The differential cross sections $d^2\sigma/d\Omega\, dT_\pi$ of π^+ and π^- at each production angle shown in Figs. 6–10 are peaked at higher energies $T_\pi(\sigma_{max})$ for positive pions than for negative pions for nuclei above aluminum. This shift of the energy distributions was also observed in the 730-MeV data of Ref. 17 and was not reproduced by the theoretical model.[19,20] The difference in peak energies $T_\pi(\sigma_{max})$ between lead and copper for positive pions (~+8 MeV) appears to reverse its sign for negative pions. This may be due to the Coulomb force between the emitted pions and the nuclear protons. The magnitude and sign of these differences are in agreement with those expected from a

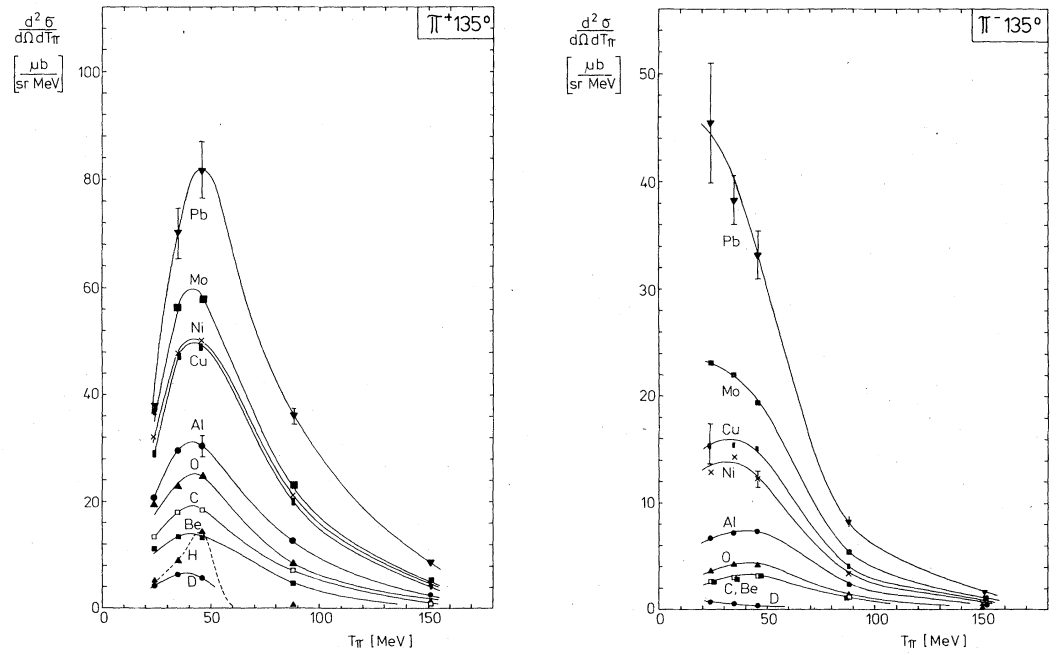

FIG. 10. As Fig. 6: production angle $\theta_\pi = 135°$.

TABLE I. Results of our measurements for carbon; results for all ten elements of the experiment are made available in PAPS; see Ref. 26. All quantities are in lab system. θ_π: pion production angle; T_π: kinetic energy of produced pions; $d^2\sigma/d\Omega dT_\pi$: differential pion production cross section of one nucleus, for unpolarized incident protons; P: asymmetry parameter, see text (Sec. V); $e/(\pi+\mu_l)$: ratio of particle rates, see text (Sec. V).

θ_π (deg)	$\pi^\pm$	T_π (MeV)	$d^2\sigma/d\Omega dT$ [μb/(sr MeV)]	P	$e/(\pi+\mu_l)$
22.5	π^+	24	6.3 ± 1.0	−0.21 ± 0.13	0.88 ± 0.12
		35	8.37 ± 0.80	−0.240 ± 0.060	0.213 ± 0.021
		88	19.2 ± 1.4	−0.111 ± 0.021	0.017 0 ± 0.001 3
		151	29.7 ± 1.4	−0.018 ± 0.017	0.009 69 ± 0.000 77
		254	24.13 ± 0.90	0.131 ± 0.023	0.004 79 ± 0.000 76
	π^-	24	1.82 ± 0.32	0.12 ± 0.22	3.43 ± 0.44
		35	2.39 ± 0.23	−0.29 ± 0.11	1.028 ± 0.059
		88	3.90 ± 0.22	−0.160 ± 0.029	0.107 5 ± 0.004 4
		151	4.30 ± 0.18	−0.162 ± 0.019	0.030 4 ± 0.001 7
		254	1.975 ± 0.090	−0.137 ± 0.028	0.005 7 ± 0.001 5
45.0	π^+	24	6.30 ± 0.90	−0.17 ± 0.13	0.565 ± 0.055
		35	9.90 ± 0.90	−0.260 ± 0.060	0.127 8 ± 0.009 3
		88	21.0 ± 1.5	−0.225 ± 0.019	0.011 5 ± 0.001 0
		151	17.49 ± 0.85	−0.079 ± 0.019	0.007 32 ± 0.000 85
		192	14.04 ± 0.69	0.063 ± 0.022	0.004 01 ± 0.000 79
	π^-	24	1.78 ± 0.35	−0.01 ± 0.31	2.52 ± 0.33
		35	2.89 ± 0.22	−0.05 ± 0.10	0.577 ± 0.034
		88	3.51 ± 0.21	−0.180 ± 0.034	0.053 8 ± 0.004 0
		151	2.72 ± 0.13	−0.124 ± 0.032	0.021 9 ± 0.002 6
		192	1.767 ± 0.091	−0.108 ± 0.033	0.005 8 ± 0.002 2
60.0	π^+	24	7.5 ± 1.2	−0.158 ± 0.082	0.396 ± 0.027
		35	11.53 ± 0.97	−0.200 ± 0.039	0.083 5 ± 0.004 9
		46	11.9 ± 1.2	−0.221 ± 0.038	0.035 7 ± 0.003 0
		88	17.94 ± 0.81	−0.193 ± 0.020	0.008 90 ± 0.000 89
		151	11.60 ± 0.44	−0.081 ± 0.016	0.004 37 ± 0.000 55
	π^-	24	1.89 ± 0.33	−0.23 ± 0.22	2.03 ± 0.21
		35	2.67 ± 0.22	−0.120 ± 0.094	0.491 ± 0.029
		46	2.79 ± 0.24	−0.122 ± 0.051	0.219 ± 0.011
		88	3.34 ± 0.17	−0.104 ± 0.034	0.043 1 ± 0.003 7
		151	1.746 ± 0.081	−0.115 ± 0.040	0.009 4 ± 0.002 7
90.0	π^+	24	11.0 ± 1.6	−0.109 ± 0.045	0.189 6 ± 0.008 1
		35	15.0 ± 1.1	−0.082 ± 0.022	0.040 1 ± 0.002 2
		46	14.8 ± 1.1	−0.100 ± 0.027	0.012 8 ± 0.001 2
		88	14.28 ± 0.57	−0.048 ± 0.013	0.003 99 ± 0.000 47
		151	4.35 ± 0.22	−0.017 ± 0.015	0.004 53 ± 0.000 64
	π^-	24	2.39 ± 0.35	0.04 ± 0.13	1.084 ± 0.070
		35	3.11 ± 0.21	−0.101 ± 0.047	0.248 ± 0.010
		46	3.28 ± 0.23	−0.088 ± 0.039	0.131 9 ± 0.006 1
		88	2.32 ± 0.10	−0.034 ± 0.024	0.026 2 ± 0.002 2
		151	0.552 ± 0.030	−0.023 ± 0.035	0.008 5 ± 0.003 3
135.0	π^+	24	13.6 ± 1.8	−0.031 ± 0.031	0.089 0 ± 0.004 3
		35	17.9 ± 1.0	0.030 ± 0.027	0.015 9 ± 0.001 9
		46	18.1 ± 1.2	−0.016 ± 0.030	0.003 6 ± 0.001 2
		88	7.14 ± 0.30	−0.082 ± 0.013	0.003 03 ± 0.000 51
		151	1.320 ± 0.094	−0.105 ± 0.020	0.005 2 ± 0.001 4
	π^-	24	2.63 ± 0.35	−0.02 ± 0.11	0.653 ± 0.040
		35	3.02 ± 0.18	−0.046 ± 0.048	0.168 8 ± 0.008 5
		46	3.23 ± 0.21	−0.003 ± 0.049	0.069 4 ± 0.005 6
		88	1.162 ± 0.050	−0.024 ± 0.035	0.018 2 ± 0.003 4
		151	0.231 ± 0.020	−0.022 ± 0.056	0.008 8 ± 0.008 4

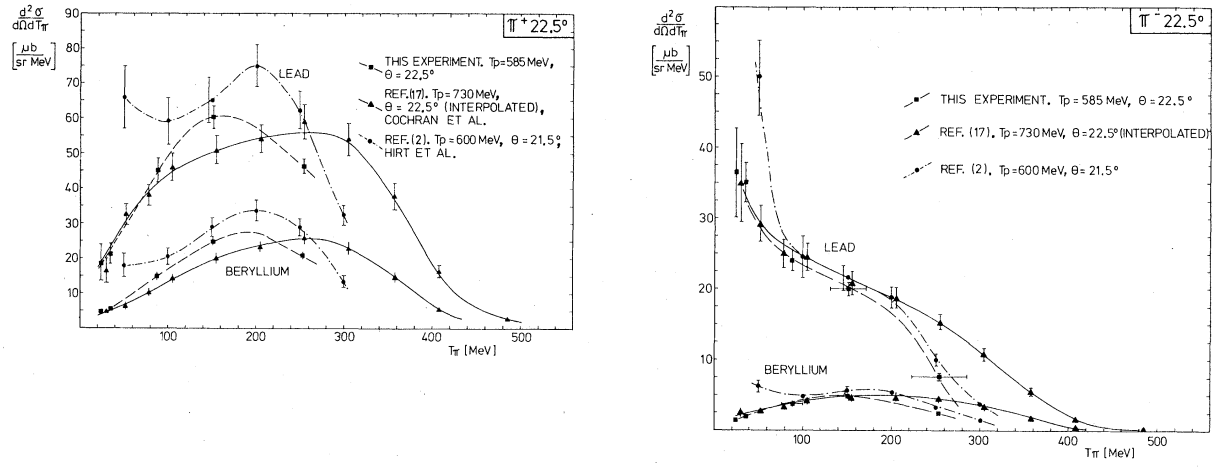

FIG. 11. Comparison of our measured differential cross sections $d^2\sigma/d\Omega dT_\pi$ for π^+ and π^- production from lead and beryllium at $T_p = 585$ MeV and $\theta_\pi = 22.5°$, with other experiments in the same proton energy region. The curves have been hand drawn through the points.

TABLE II. Total cross sections for the production of charged pions by protons with $T_p = 585$ MeV. The quantity $\sigma_T(\pi^+)/Z^{1/3}$, where Z is the nuclear charge number, is roughly independent of Z for nuclei heavier than oxygen, and the analog is true for $\sigma_T(\pi^-)/N^{2/3}$ for nuclei heavier than beryllium.

Target	$\sigma_T(\pi^+)$ (mb)	$\sigma_T(\pi^-)$ (mb)	$\frac{\sigma_T(\pi^+)}{Z^{1/3}}$ (mb)	$\frac{\sigma_T(\pi^-)}{N^{2/3}}$ (mb)
Pb	86 ± 11	41.5 ± 5.1	19.8 ± 2.5	1.66 ± 0.20
Mo	69.6 ± 8.5	24.5 ± 3.0	20.1 ± 2.4	1.72 ± 0.21
Cu	60.0 ± 7.4	18.0 ± 2.2	19.5 ± 2.4	1.70 ± 0.21
Ni	62.5 ± 7.7	14.7 ± 1.8	20.6 ± 2.5	1.50 ± 0.18
Al	43.8 ± 5.4	9.8 ± 1.2	18.6 ± 2.3	1.68 ± 0.20
O	34.6 ± 4.2	6.40 ± 0.79	17.3 ± 2.1	1.61 ± 0.20
C	28.5 ± 3.5	4.72 ± 0.58	15.7 ± 1.9	1.43 ± 0.18
Be	22.7 ± 2.8	4.75 ± 0.59	14.3 ± 1.8	1.62 ± 0.20
D	8.7 ± 1.1	1.03 ± 0.13	8.7 ± 1.1	1.03 ± 0.13
H	9.7 ± 1.2		9.7 ± 1.2	

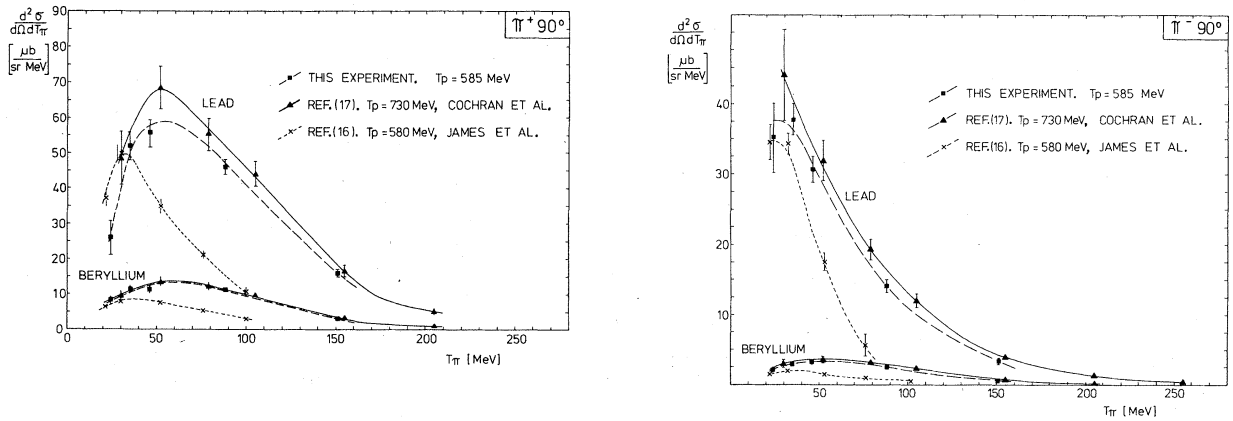

FIG. 12. As Fig. 11: production angle $\theta_\pi = 90°$.

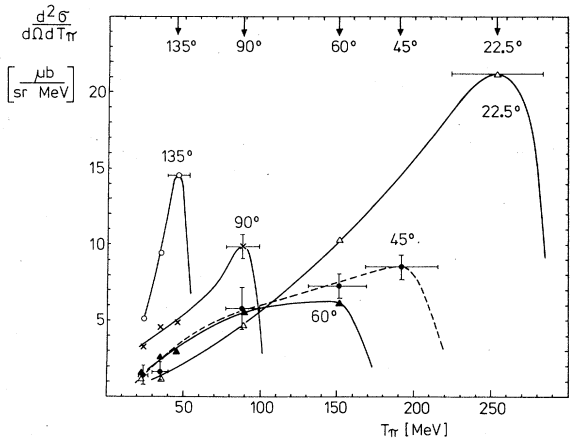

FIG. 13. The measured differential cross sections $d^2\sigma/d\Omega dT_\pi$ for π^+ production from hydrogen by 585-MeV protons at $\theta_\pi = 22.5$, 45, 60, 90, and 135° in the laboratory. The pion energies T_π corresponding to the energy of the pion in the $pp \rightarrow d\pi^+$ reaction at the various lab angles are indicated at the top of the diagram. The sharp peaks in the differential cross section at these energies due to this reaction are broadened by our large momentum acceptance. The corresponding kinetic energy acceptance at each lab angle is indicated on the data points.

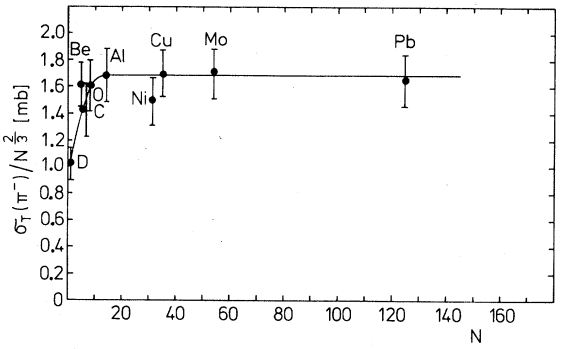

FIG. 15. Measured total production cross sections for negative pions from various nuclei divided by $N^{2/3}$ plotted against the nuclear neutron number N.

simple model[24] with uniform nuclear charge distributions and the radii of Ref. 19.

The comparisons of our data with those of Hirt *et al.*,[2] Cochran *et al.*,[17] and James *et al.*[16] show several interesting features (e.g., see Figs. 11 and 12). In the case of π^+ our cross sections are lower than those of Ref. 2, particularly at their lowest pion energy. The agreement with the π^- data of Ref. 2 is good except again at their lowest pion energy. Our data agree with those of James *et al.*[16] for $T_\pi \leq 35$ MeV, but for higher pion energies, the experiments are in strong disagreement. Comparing our pion production cross sections for 585-MeV incident protons with those of Cochran *et al.*[17] for 730-MeV protons indicates that for pion energies

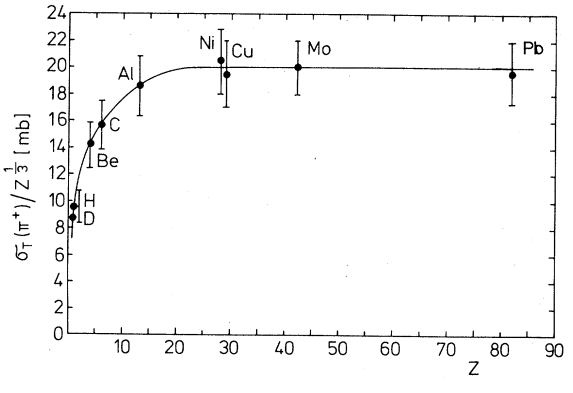

FIG. 14. Measured total pion production cross sections for positive pions from various nuclei divided by $Z^{1/3}$ plotted as a function of the nuclear charge Z. Our experimental results are plotted as points with error bars; the curve is drawn to guide the eye. The errors shown are the total uncertainties.

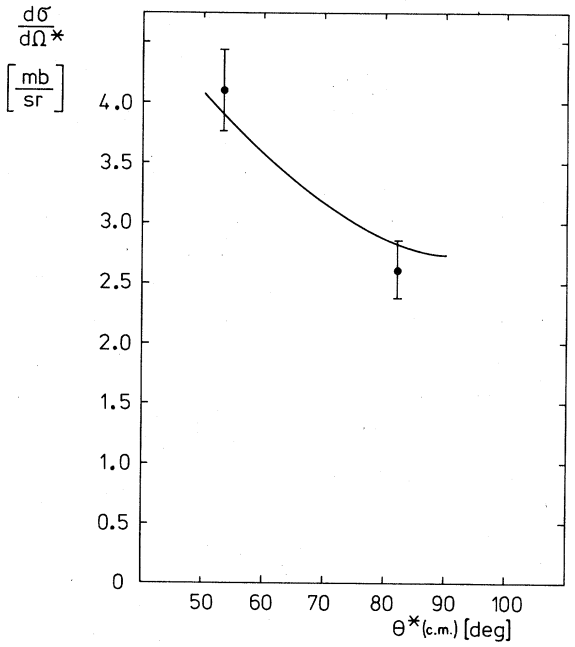

FIG. 16. Results of the proton-proton differential elastic scattering cross section measurement. The measured differential cross sections (in the center of mass system) are plotted as points with error bars. The curve is the prediction derived from the Saclay nucleon-nucleon phase shifts (Ref. 25) at $T_p = 585$ MeV.

TABLE III. Results of the proton-proton differential elastic scattering cross section, in the c.m. system, and asymmetry check at $T_p = 585$ MeV. Columns 2 and 4: our results. Columns 3 and 5: values calculated from the Saclay phase shifts (Ref. 25).

Lab angle	Cross section $d\sigma/d\Omega^*$ (mb/sr) This experiment	Saclay	Asymmetry parameter P This experiment	Saclay
60°	4.10 ± 0.34	3.90 ± 0.04	0.454 ± 0.027	0.472 ± 0.050
45°	2.61 ± 0.24	2.86 ± 0.06	0.116 ± 0.023	0.115 ± 0.040

below 150 MeV, these cross sections differ little from each other for all pion production angles. The advantages of using higher energy protons than 585 MeV become evident at pion production angles smaller than 45°, where higher energy pions become available.

The differential cross sections $d^2\sigma/d\Omega dT_\pi$ for π^+ production from hydrogen at production angles $\theta_\pi = 22.5°$, 45°, 60°, 90°, and 135° are shown in Fig. 13. For each θ_π, the pion energy corresponding to the $pp \to d\pi^+$ reaction is indicated. In every case the energy distribution is peaked at the en-

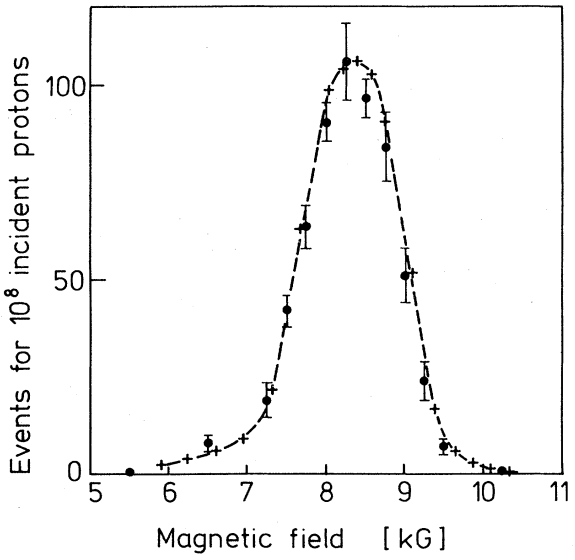

FIG. 17. Proton-proton scattering rates for unpolarized protons as a function of the magnetic field in the center of the spectrometer magnet, placed at θ(lab) = 60°. The experimental rates are plotted as crosses (typical statistical uncertainty ~1%). The results of the Monte Carlo computer program are shown as circles with error bars. The differential p-p scattering cross section used in the Monte Carlo program was calculated from the Saclay phase shifts (Ref. 25). A curve has been hand drawn through the experimental points. The Monte Carlo points are seen to agree with the experimental points. This represents a check of the monitoring and the acceptance calculation.

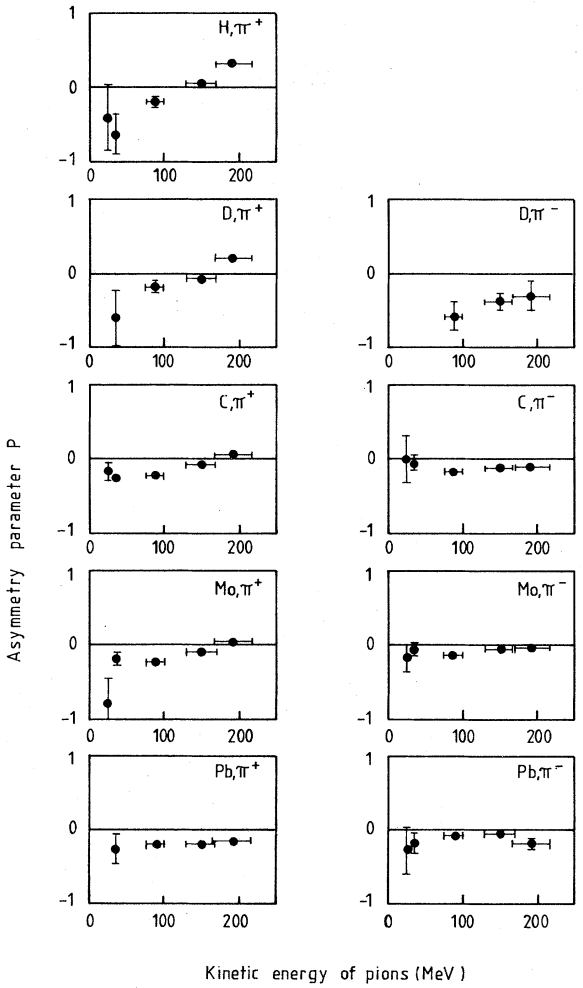

FIG. 18. Measured asymmetry parameters P in charged pion production from various elements by 585 MeV polarized protons at a production angle θ_π of 45°; see text Sec. V.

ergy corresponding to this reaction, in contrast to the data of Ref. 17 at 730 MeV, where no clear enhancements were observed. This can be understood because of the increased importance of the $pp \to d\pi^+$ channel at our incident proton energy, near which the total cross section for this reaction has its peak.[27] A complete theoretical model for pion production from nuclei at an energy near 600 MeV should include the contribution from this reaction. The energy distributions of Fig. 13 have been integrated over energy and angle to give a total π^+ production cross section of 9.7 ± 1.0 mb, in agreement with the sum of total cross sections for the reactions $pp \to pn\pi^+$ and $pp \to d\pi^+$ at 585 MeV from Ref. 27. Our integrated total cross section for π^+ production from deuterium is 8.7 ± 1.1 mb. The most probable value of this cross section is thus smaller than that from hydrogen as also observed by Cochran *et al.*[17] at 730 MeV, who attributed the fact to strong interference and/or shadowing.

Our total cross sections σ_T for π^+ and π^- production at 585-MeV proton kinetic energy are listed in Table II. The dependence of $\sigma_T(\pi^+)/Z^{1/3}$ and $\sigma_T(\pi^-)/N^{2/3}$ on Z and N, respectively, are presented in Figs. 14 and 15 and also in Table II. The total cross sections for π^+ and π^- production from nuclei above carbon show the $Z^{1/3}$ and $N^{2/3}$ dependence, respectively, as expected from theoretical arguments[19,20] including the effects of strong pion absorption in both cases and π^0 charge exchange in the latter case. The ratio of the total cross sections for π^+ and π^- production are in good agreement with the predictions of the isobar model of Silbar and Sternheim.[19,20]

The results of our proton-proton scattering measurements are presented in Table III and in Fig. 16 together with the predictions derived from the Saclay phase shifts.[25] The predictions quoted in Table III and shown in Fig. 16 were obtained with an interpolation between fits to two sets of experimental proton-proton scattering data at very nearby energies, namely 582 and 593 MeV.[28,29] Both sets of differential cross section data were well reproduced by the phase shifts[25] used for our interpolation. The Monte Carlo and experimental proton-proton scattering rates as a function of the magnetic field of the spectrometer are plotted in Fig. 17 for a laboratory scattering angle of 60°. The two curves in Fig. 17 agree within the statistical uncertainties, indicating that the overall acceptance and monitoring of our system is correctly estimated in our Monte Carlo program.

The polarization parameters P in pion production from carbon measured in our experiment are listed in Table I. Some of the data from other nuclei are shown in Fig. 18. The polarization parameters are in general quite small, particularly for negative pions. Since a large fraction of the negative pions are not produced directly but rather by charge exchange of neutral pions, any polarization dependence of the π^- production is expected to be small. On the other hand, positive pions which are predominantly produced in a single pion production process within the nucleus might be expected to show a larger polarization sensitivity than negative pions, and this is confirmed by our data.

ACKNOWLEDGMENTS

We would like to thank M. Byrne, N. Fischer, P. Gheno, S. Jaccard, B. Jost, and D. Rapin for their contributions during the setting up and running of the experiment. Thanks are also due to J. Domingo, L. Dubal, D. C. George, H. -J. Gerber, W. Hirt, P. Schwaller, and G. Vecsey for discussions. The experiment would not have been possible without the excellent technical support of many groups at SIN.

---

*Present address: Physics Department, Stanford University, Stanford, California 94305.

†Present address: Marconi Space and Defence Systems, The Grove, Warren Lane, Stanmore, Middlesex HA7 4 LY, England.

‡Present address: Landis and Gyr AG, CH-6300 Zug, Switzerland.

[1]R. Haddock, M. Zeller, and K. Crowe, UCLA Report No. UCLA-34P106 (unpublished).

[2]W. Hirt, E. Heer, M. Martin, E. G. Michaelis, C. Serre, P. Skarek, and B. T. Wright, CERN Report No. 69-24 (unpublished).

[3]B. Baldoni, S. Focardi, H. Hromadnik, L. Monari, F. Saporetti, S. Feminò, F. Mezzanares, E. Bertolini, and G. Gialanella, Nuovo Cimento 26, 1376 (1962).

[4]V. M. Guzhavin, G. K. Kliger, V. Z. Kolganov, A. V. Lebedev, K. S. Marish, Yu. D. Prokoshkin, V. T. Smolyankin, A. P. Sokolov, L. M. Soroko, and Ts'ui Wa-Ch'uang, Zh. Eksp. Teor. Fiz. 46, 1245 (1964) [Sov. Phys.—JETP 19, 847 (1964)].

[5]D. V. Bugg, A. J. Oxley, J. A. Zoll, J. G. Rushbrooke, V. E. Barnes, J. B. Kinson, W. P. Dodd, G. A. Doran, and L. Riddiford, Phys. Rev. 133, B1017 (1964).

[6]B. S. Neganov and O. V. Savchenko, Zh. Eksp. Teor. Fiz. 32, 1265 (1957) [Sov. Phys.—JETP 5, 1033 (1957)].

[7]M. G. Meshcheriakov, V. P. Zrelov, B. S. Neganov, I. K. Vzorov, and A. F. Shabudin, Zh. Eksp. Teor. Fiz. 31, 45 (1956) [Sov. Phys.—JETP 4, 60 (1957)].

[8]A. G. Meshkovskii, Iu. S. Pligin, Ya. Ya. Shalamov, and V. A. Shebanov, Zh. Eksp. Teor. Fiz. 31, 560 (1956) [Sov. Phys.—JETP 4, 404 (1957)].

[9]V. M. Sidorov, Zh. Eksp. Teor. Fiz. 31, 178 (1956) [Sov. Phys.—JETP 4, 22 (1957)].

[10]Yu. A. Batusov, N. I. Kostanashvili, G. I. Lebedevich,

D. S. Nabichvrishvili, and V. A. Yarba, Yad. Fiz. 10, 805 (1969) [Sov. J. Nucl. Phys. 10, 465 (1970)].
[11]E. Lillethun, Phys. Rev. 125, 665 (1962).
[12]M. G. Meshcheriakov, I. K. Vzorov, V. P. Zrelov, B. S. Neganov, and A. F. Shabudin, Zh. Eksp. Teor. Fiz. 31, 55 (1956) [Sov. Phys.—JETP 4, 79 (1957)].
[13]A. G. Meshkovskii, Iu. S. Pligin, Ya. Ya. Shalamov, and V. A. Shebanov, Zh. Eksp. Teor. Fiz. 31, 987 (1956) [Sov. Phys.—JETP 4, 842 (1957)]; 32, 1328 (1957) [5, 1085 (1957)].
[14]A. G. Meshkovskii, Ya. Ya. Shalamov, and V. A. Shebanov, Zh. Eksp. Teor. Fiz. 33, 602 (1957) [Sov. Phys.—JETP 6, 463 (1958)].
[15]A. G. Meshkovskii, Ya. Ya. Shalamov, and V. A. Shebanov, Zh. Eksp. Teor. Fiz. 34, 1426 (1958) [Sov. Phys.—JETP 7, 987 (1958)].
[16]P. W. James, D. A. Bryman, G. R. Mason, L. P. Robertson, J. S. Vincent, and T. R. Witter, TRIUMF Report No. VPN-75-1, 1975 (unpublished).
[17]D. R. F. Cochran, P. N. Dean, P. A. M. Gram, E. A. Knapp, E. R. Martin, D. E. Nagle, R. B. Perkins, W. J. Shlaer, H. A. Thiessen, and E. B. Theriot, Phys. Rev. D 6, 3085 (1972).
[18]J. Crawford, M. Daum, G. H. Eaton, R. Frosch, J. McCulloch, F. Pozar, E. Steiner, R. Hess, and D. Werren, SIN-Report No. PR-77-001, 1977 (unpublished).
[19]Morton M. Sternheim and Richard R. Silbar, Phys. Rev. D 6, 3117 (1972).
[20]Richard R. Silbar and Morton M. Sternheim, Phys. Rev. C 8, 492 (1973).
[21]M. Daum, SIN-Report No. TM-09-45, 1976 (unpublished).
[22]D. Rapin, thesis, University of Geneva, 1978 (unpublished).
[23]G. H. Eaton and F. Pozar, SIN-Report No. TM-33-02, 1975 (unpublished).
[24]R. Horisberger, Diplomarbeit, ETH Zurich, 1979 (unpublished).
[25]Saclay Nucleon-Nucleon Phase Shift compilation, F. Lehar, private communication (1979).
[26]See AIP document No. PAPS PRVCA-22-1184-13 for ten pages of tables of measured differential pion production cross sections, asymmetry parameters, and electron contaminations for all elements studied (see abstract). Order by PAPS number and journal reference from American Institute of Physics, Physics Auxiliary Publications Service, 335 East 45th Street, New York, New York 10017. The prices are $1.50 for microfiche or $5 for photocopies. Airmail additional. Make checks payable to the American Institute of Physics. This material also appears in *Current Physics Microfilm*, the monthly microfilm edition of the complete set of journals published by AIP, on frames immediately following this journal article.
[27]Compilation of p and $\bar{p}$ induced reaction cross sections, E. Bracci, J. P. Droulez, E. Flaminio, J. D. Hansen, and D. R. O. Morrison, CERN Report No. CERN/HERA 73-1, 1973 (unpublished).
[28]E. T. Boschitz, W. K. Roberts, J. S. Vincent, M. Blecher, K. Gotow, P. C. Gugelot, C. F. Perdrisat, L. W. Swenson, and J. R. Priest, Phys. Rev. C 6, 457 (1972).
[29]K. Abe, B. A. Barnett, J. H. Goldman, A. T. Laasanen, P. H. Steinberg, G. F. Marmer, D. R. Moffett, and E. F. Parker, Phys. Rev. D 12, 1 (1975). M. G. Albrow, S. Andersson/Almehed, B. Bošnjaković, C. Daum, F. C. Erné, J. P. Lagnaux, J. C. Sens, and F. Udo, Nucl. Phys. B23, 445 (1970).